energies

Article

Challenges of Large Converter-Fed Synchronous Machines for Variable-Speed Pumped Hydro Storage

Stefan Polster [1,*], Johannes Deschler [2], Herwig Renner [3], Aurelie Bocquel [4] and Martin Janssen [4]

[1] Verbund Hydro Power GmbH, 1010 Vienna, Austria
[2] Grenzkraftwerke GmbH, 84359 Simbach, Germany; johannes.deschler@verbund.com
[3] Institute of Electric Power Systems, Graz University of Technology, 8010 Graz, Austria; herwig.renner@tugraz.at
[4] GE Power Conversion Berlin, 12277 Berlin, Germany; aurelie.bocquel@ge.com (A.B.); martin.janssen@ge.com (M.J.)
* Correspondence: stefan.polster@verbund.com

Abstract: The green energy transition of electrical energy production is leading to an increasing share of total energy production for volatile renewable energy sources, mainly wind and solar power. To handle this volatile production, flexible and efficient energy storage is required. The development of high-power converters has enabled the generation of variable-speed pumped hydro storage power plants, combining the so-far-unequalled energy storage capacity of classical pumped-storage hydro power plants and the recently increased operation requirements. The introduction of large-scale converters has led to new challenges in the overall design of power plant systems. This paper intended to take a closer look at a large-scale converter-fed synchronous generator, especially the distribution of the current and voltage harmonics caused by the converter in the implemented generation system. Thereby, holistic design considerations for an ideal loss distribution as well as possible measures to limit the effects of harmonic coupling at the generator shaft and bearings are discussed. Furthermore, basic considerations of harmonic emission to the connected network are described. These topics are addressed by analyzing on-site measurements at an 85 MVA converter-fed synchronous generator with a voltage source inverter, underpinned with the theoretical background.

Keywords: converter-fed synchronous machines; voltage source inverter; shaft voltage; harmonic emission; variable-speed pumped hydro storage

Citation: Polster, S.; Deschler, J.; Renner, H.; Bocquel, A.; Janssen, M. Challenges of Large Converter-Fed Synchronous Machines for Variable-Speed Pumped Hydro Storage. *Energies* **2023**, *16*, 7506. https://doi.org/10.3390/en16227506

Academic Editor: José Gabriel Oliveira Pinto

Received: 29 September 2023
Revised: 31 October 2023
Accepted: 1 November 2023
Published: 9 November 2023

1. Introduction

The concept of variable-speed hydro storage power plants has been discussed in the literature for quite a long time, for example, in [1–5]. The speed variability offers an increase in the turbine efficiency, especially if the net head changes significantly, as well as an improved operational flexibility [6–9]. Several publications have addressed sophisticated control approaches for variable-speed power plants, focusing on grid support [10–13] and modeling approaches [14,15].

The implementation of variable-speed hydro storage power plants is based on two different designs. The double-fed induction generator (DFIG) is already in operation in several large-scale power plants such as Goldisthal [16,17], Frades II [18,19], and Linth–Limmern [20]. The second applied technology is the converter-fed synchronous machine (CFSM) with a 50 Hz bypass, currently in operation in the power plants Grimsel II [21], Malta Oberstufe [22,23], and Limberg I.

This paper focuses on the practical challenges occurring in a CFSM system. The addressed challenges can be separated in two thematic groups. The first focuses on the selection of the pulse pattern and number of pulses per half wave. Thereby, the emission of voltage and current harmonics in the CFSM system and at the PCC, as well as the optimization of the converter losses, have to be considered. In general, an increased number of pulses decreases the harmonic emission of the converter but leads to higher switching losses. The second group deals with the auxiliary electrical design and control challenges for reliable operation. Therefore, the necessary electric coordination of the generator current and voltage and the operational limits of measurement transducers are discussed, and measures to reduce the occurring high-frequency shaft voltage are examined.

The content of this paper is based on design considerations and measurements at the CFSM-based pumped-storage hydro power plant Limberg I, located at the dam on the "Wasserfallboden" reservoir in Kaprun. Limberg I has two turbine groups and was refurbished in 2021 and 2022 to reach 80 MW pump and turbine power per CFSM system.

Table 1 gives the main parameters for a single system.

Table 1. Main parameters of one turbine group of Limberg I.

Power range pump operation [1]	35–80 MW
Power range turbine operation [1]	9–80 MW
Speed range	400–750 rpm
Stator frequency range	0–50 Hz
Number of pole pairs	4
Active power gradient	up to 2 MW/s
Change over time [2]	<60 s
Rated converter power	4×21.25 MVA

[1] Power range depends on the net head. [2] Times measured during commissioning.

The used converter concept and the selection considerations on the utilized pulse pattern are discussed in Section 2. The practical effects of variable-speed operation on the measurement transducers in the converter–generator connection are shown in Section 3. The basic model of the grid to evaluate the effects of the harmonic emission is described in Section 4. Sections 5 and 6 focus on the analysis of harmonic measurements in the CFSM system of Limberg I and the occurring high-frequency shaft voltage.

2. Converter Concept and Pulse Pattern Selection

The fully fed converter solution implemented in Limberg I to drive the pump turbine was designed to be integrated into the historical Limberg I power plant. It consists of a main medium-voltage press pack injection-enhanced gate transistor (IEGT) converter (MV7000) connected to the stator of the electrical machine, and a static excitation thyristor bridge converter connected to the rotor. The thyristor bridge controls the rotor current and contributes to the flux control of the machine. The full electrical power flow generated by the electrical machine is converted and fed into the grid by the MV7000 converter via a transformer; see Figure 1. The converter is built of four parallel units. The units on the machine side are connected in parallel. The units on the grid side are connected to a five-winding transformer. Two pre-charge transformers are used to pre-charge the dc links. One of them is necessary and the second one is redundant. This redundancy allows a three out of four operation regardless of a failed converter unit.

For this application, a trade-off had to be found considering the main constraints:

- As for other retrofit projects, the converter had to be integrated into the historical building that was designed for a smaller power at a time without converter technology. Therefore, a small footprint of 90 m^2 and a high power density were required. The power density achieved is 246 kW/m^3. Figure 2 shows a picture of the machine hall and the built, fully enclosed, converter.
- The voltage level of the machine and the converter have to match. The converter can adjust to a lower machine voltage, but a high efficiency will only be achieved if the full voltage range of the converter is utilized.
- The frequency range of the converter should match the stator frequency range of the generator. Especially in the frequency range above 40 Hz, some converter solutions can be limited. The MV7000 can operate at full power typically up to 60 Hz. Thus, the

speed range of the pump-turbine and the converter technology set design limitations for the generator.
- The grid requirements have to be fulfilled. Especially the level of harmonic distortions must be kept below the limits of the applicable grid code. Additionally, the required PQ diagram at the point of common coupling (PCC) has a significant impact on the system design. The transformer should be designed so that the parallel units can be operated independently. Then, harmonic cancellation between the individual units is possible.
- For a high efficiency, the overall losses in the converter–generator system have to be minimized. Usually, a low IEGT switching frequency is chosen to reduce the converter losses. But this may increase the generator losses.
- The amount of distortion of the stator current impacts the losses in the machine and the heating of the generator. A trade-off between the converter losses and the amount of distortion of the stator current, and thus, the generator losses over the frequency range, has to be found.
- The rate of change in the stator voltage has to be limited. Usually, a filter is used to limit the $\mathrm{d}v/\mathrm{d}t$ of switching and the impact on the machine.
- A standard converter design should be used to optimize costs and has to be adapted to the requirements of the project.

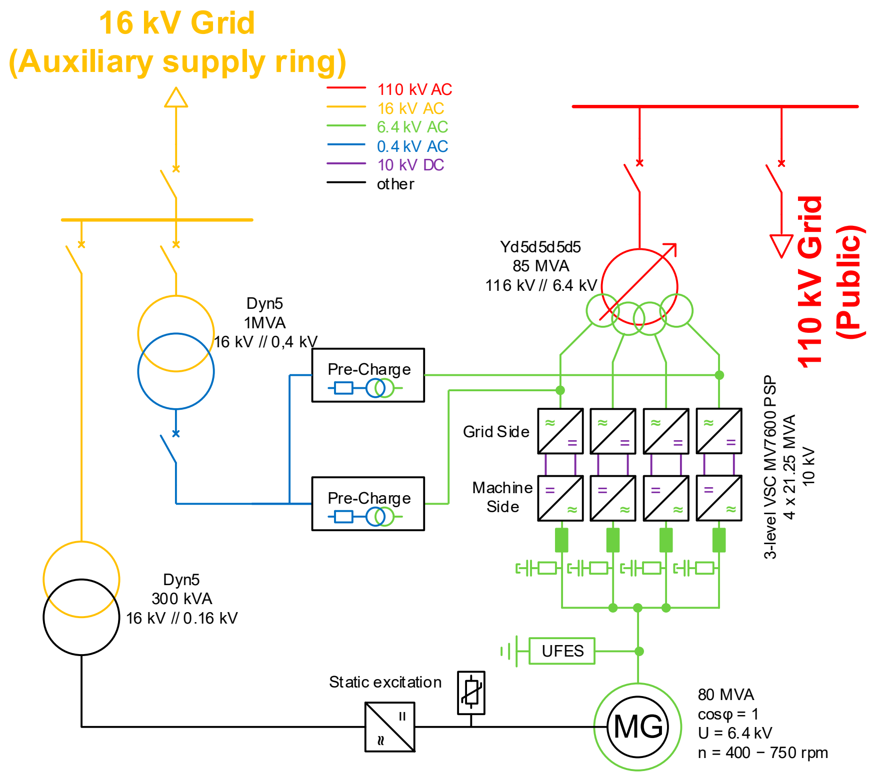

Figure 1. Single-line diagram of one CFSM unit in Limberg I. UFES refers to ultra-fast earthing switch.

Based on these constraints, the chosen voltage level was 6 kV and a solution with four modules of MV7600 was chosen. This converter is a neutral-point-clamped (NPC) converter with a dc link kept at a constant voltage of 10 kV which acts on the grid side and on the machine side as a three-level converter. It is realized by the series connection of two press pack IEGTs per branch, which is a very robust technology. In [24], there are some insights into the MV7000 NPC technology. Figure 3 shows the configuration of an MV7600 module.

Figure 2. Historical machine hall of power plant Limberg I with two power trains after refurbishment in the years 2021 and 2022. Reprinted with permission from GE Power Conversion 2023.

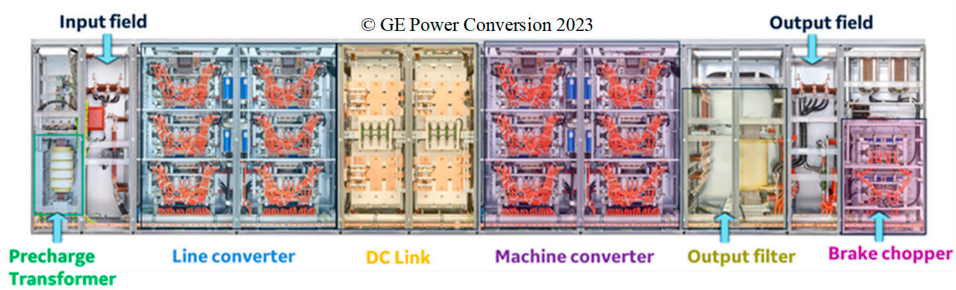

Figure 3. Overview of an MV7600 converter module. Reprinted with permission from GE Power Conversion 2023.

Once the hardware is fixed, an important part of the system design is the selection of the pulse patterns of the converter. They can be optimized with respect to various aspects:

- Converter losses;
- Harmonics/THD;
- Impact on the grid/the machine;
- Load characteristics.

Higher pulse frequencies will improve the voltage and current quality but also lead to higher converter losses. An important factor for the maximum possible pulse frequency are the allowable losses of the semiconductors.

The correlation between converter losses and pulse frequency is very complex. The converter losses of the different parts depend on the current, voltage, power factor, and switching frequency. The split of the losses is roughly described in the following simplified equation.

$$P_{\text{loss,total}} = P_{\text{loss,DC}} + P_{\text{loss,MC}} + P_{\text{loss,LC}} + P_{\text{loss,filter}} \quad (1)$$

The indexes refer to the main parts of the converter (DC: dc link; LC: line converter; MC: machine converter). The semiconductor losses are the most important; here, $P_{\text{loss,MC}}$ and $P_{\text{loss,LC}}$. They roughly consist in the conduction losses P_{cond} and the switching losses P_{switch}.

$$P_{\text{loss}} = P_{\text{cond}} + P_{\text{switch}} \quad (2)$$

The conduction losses depend on the current. The switching losses are dependent on the pulse frequency of the converter. For example, in Equations (2)–(8) and (2)–(9) in [25], the following formulas are given to describe the losses in an IEGT:

$$P_{\text{cond}}(i) = i \cdot V_{\text{T0}} + r_{\text{T0}} \cdot i^2 \quad (3)$$

where

V_{T0}: threshold voltage;

r_{T0}: equivalent differential resistance;

i: IEGT current.

$$E_{sw}(i, V_{comm}) = A_{swX} + B_{swX} \cdot i + C_{swX} \cdot i^2 \cdot \frac{V_{comm}}{V_{base}} \tag{4}$$

where

V_{comm}: commutation voltage;

V_{base}: voltage at which the losses were measured;

A_{swX}, B_{swX}, C_{swX}: fitting constants.

Each of the losses, according to Equation (1), depend on the switching frequency. The impacts of the switching frequency are various and depend on the physics and operation mode of the considered element. For example, depending on the power factor and of the sign of the power flow the current will flow either in the IEGTs or in the diodes, which will have repercussions on the losses.

The most common modulation technique is pulse-width modulation (PWM). Figure 4 shows two different PWM types, continuous and discontinuous PWM, and the resulting harmonics of the output voltage. With continuous PWM (H3) the IEGT switchings are distributed over the whole period; with discontinuous PWM (3LC) there are no switchings within a third of the period. This method can be used to reduce the converter losses or to use a higher pulse frequency. In the example shown in Figure 4, the total semiconductor losses are reduced by approximately 3% using the discontinuous PWM compared with the continuous PWM. The different PWM types also differ in the harmonic characteristic. This can be very useful, especially for active front-end (AFE) applications, to respect the harmonic limits of the grid code.

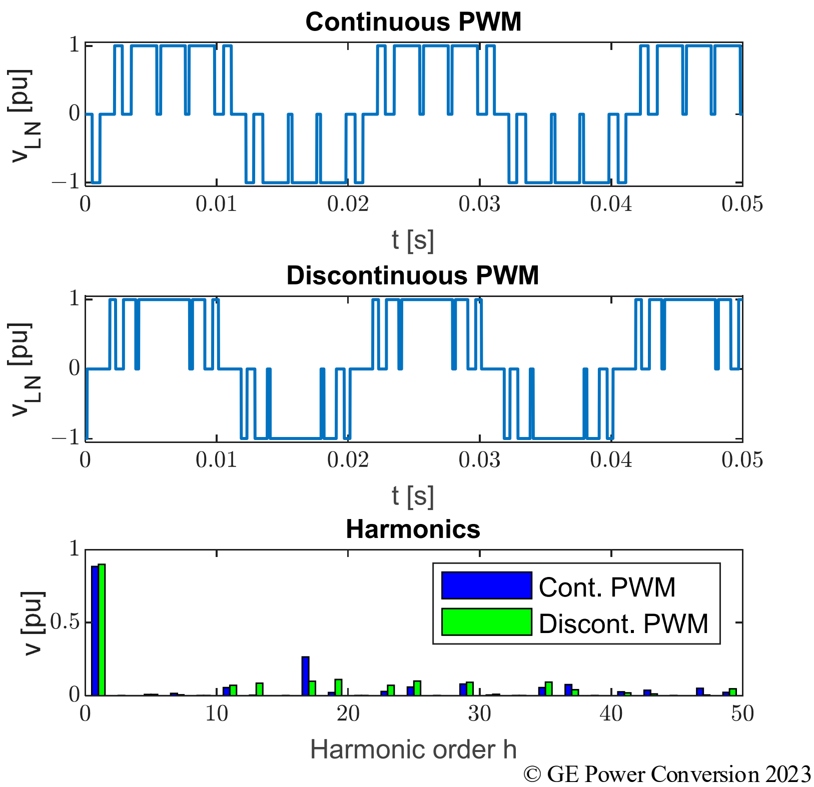

Figure 4. Comparison of pulse patterns and their harmonics for continuous PWM (H3) and discontinuous PWM (3LC). Reprinted with permission from GE Power Conversion 2023.

Pulse interleaving can be used for applications with more than one unit in parallel under the condition that the systems are decoupled. Therefore, a five-winding transformer on the grid side is chosen. Towards the grid, the system has an equivalent output voltage with a multilevel waveform of 17 levels for the line-to-line voltage, with the switching frequency increased by four, as shown in Figure 5.

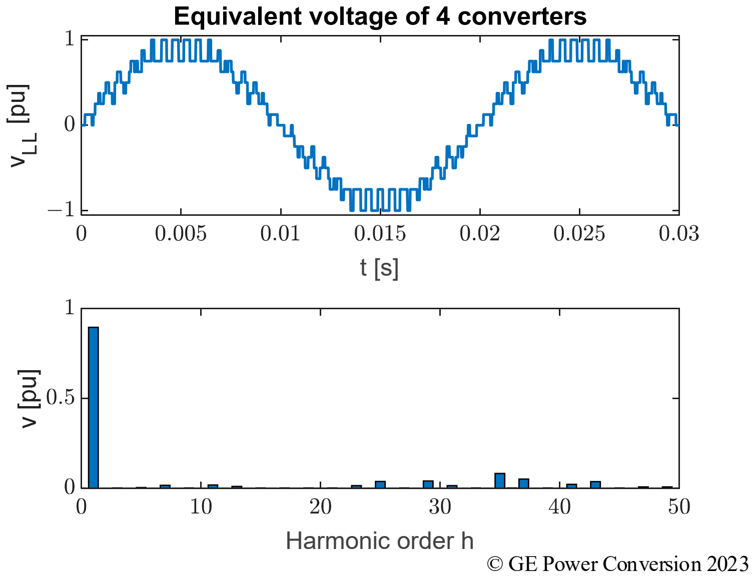

Figure 5. Equivalent voltage of four units with pulse interleaving. Reprinted with permission from GE Power Conversion 2023.

Usually synchronized pulse patterns with a given number of pulses per period are used. Figure 6 shows a comparison of different pulse numbers per half oscillation period (five, seven, and nine pulses per fundamental half period). By the increased pulse frequency, the main voltage harmonics are shifted to higher frequencies, but are still below the 100th harmonic. Therefore, the THD_u decreases only slightly. The current harmonics and the THD_i decrease significantly because the machine impedance increases linearly with increasing frequency. The drawback is the increased losses of the converter. For the shown operation point, at approximately 60% partial load, the semiconductor losses of the machine converter are approximately 17% higher with seven pulses per half period and 23% higher with nine pulses per half period than with five pulses per period. But this has to be compared to the reduced losses in the machine due to the lower current distortion. The converter–generator system has to be analyzed by considering all aspects of the complete unit to find the optimal operation mode.

Whereas the grid converter uses the same pulse pattern for the whole operation range, the pulse pattern of the machine converter changes with the operation point. The pulse frequency of the machine converter should be kept approximately constant over the speed range to assure a similar voltage and current quality over the whole speed range. This leads to a reduction in the pulse number with increasing speed; e.g., 11 pulses in the low-speed range correspond to 7 pulses at high speeds. It is possible to increase the pulse frequency due to the reduced losses for operation points with partial loads. But the advantages for other components of the system have to outweigh the increased losses of the converter.

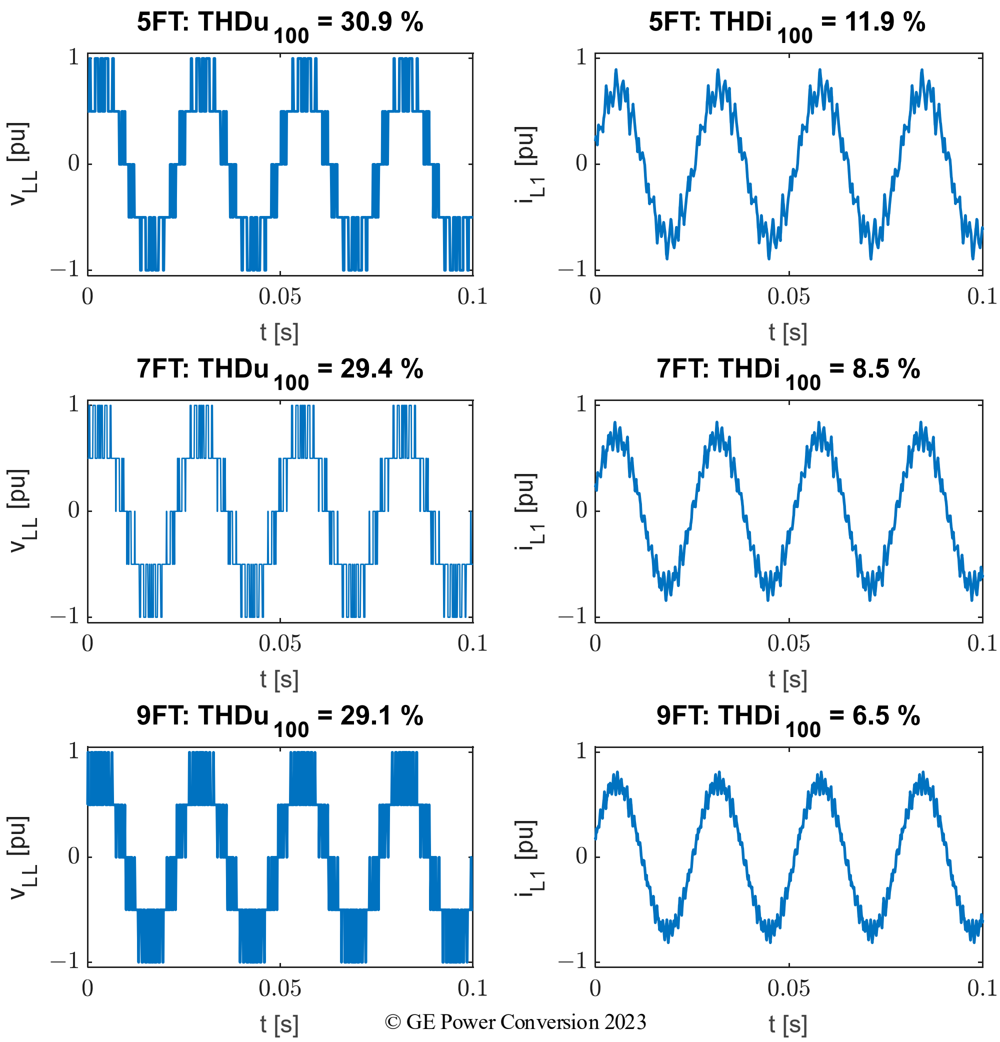

Figure 6. Comparison of 5-, 7-, and 9-fold switching. Reprinted with permission from GE Power Conversion 2023.

3. Variable-Speed Operation

Variable-speed operation is realized by regulating the stator voltage and stator current depending on the stator frequency, as shown in Figure 7. The stator current and stator voltage are reduced during the start-up operation. With this method, the short-circuit currents can be limited by reducing the magnetic flux, the saturation of the protection current transformers in the stator bars can be avoided, and voltage transformers at the stator bars will be not damaged by exceeding the maximum operation time at a specific voltage and frequency. The stator current will be increased after reaching the first operational point. The stator current limit is given by the nominal stator current. The output power of generator at a specific stator frequency is given by the stator current and stator voltage.

While the frequency converter can operate between 0 Hz and 60 Hz, variable-speed operation is usually possible in a smaller range of frequencies: typically over 10 Hz, to a nominal operation between 40 Hz and 50 Hz.

The operation at low frequencies mainly occurs during start-up and changeover for a short period of time. The changeover time from turbine to pump operation and vice versa was reduced significantly by the refurbishment of Limberg I. Changeover times of less than 1 min are sufficient to changeover from turbine to pump operation; see Figure 8.

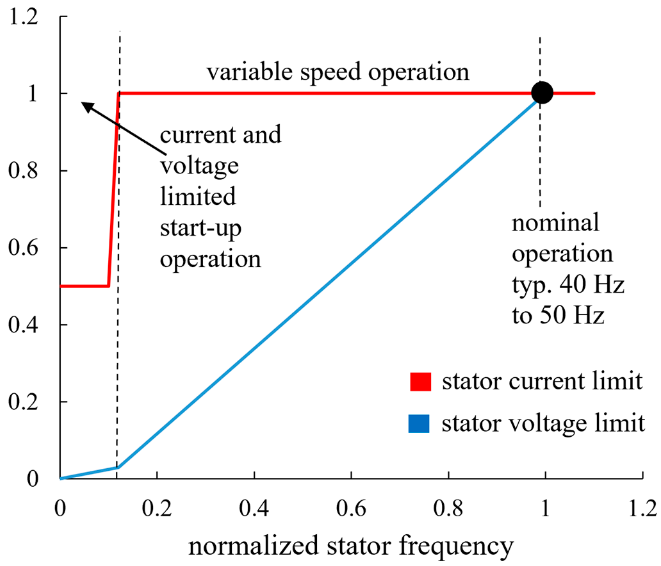

Figure 7. Example U/f- and I/f-characteristics of stator voltage and stator current.

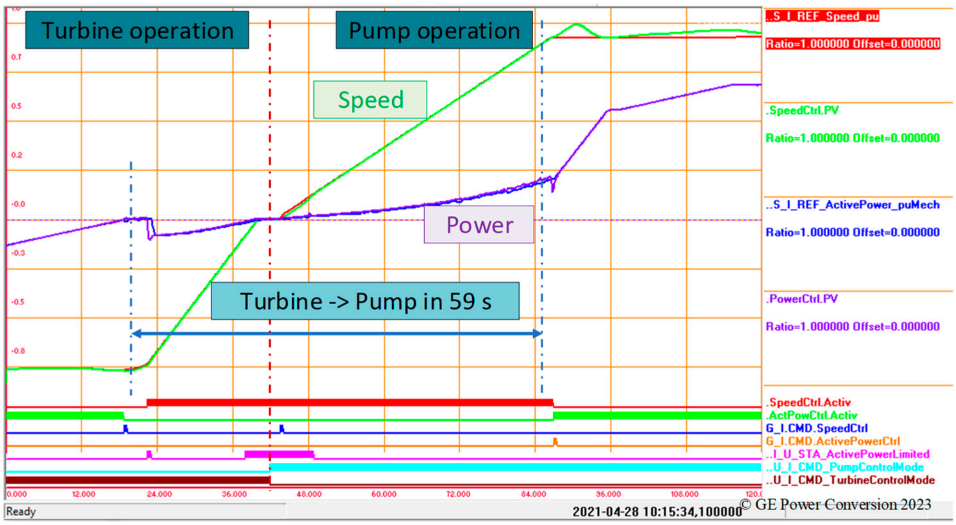

Figure 8. Measured changeover from turbine to pump operation at Limberg I. Reprinted with permission from GE Power Conversion 2023.

4. Grid Harmonics and Resonances

Considering power quality, inverter-based variable-speed generators are a source of harmonic distortion. This is a new aspect in commissioning these units since harmonics are not an issue for classical synchronous machines.

The harmonic emission level from an installation into the grid is the harmonic voltage at each harmonic frequency which would be caused by the installation at the point of evaluation, which is usually the point of connection. The classical frequency range for harmonics ends at 2500 Hz (50th harmonic). Considering the commonly used switching frequencies for high-power inverters, this frequency range is sufficient. Moreover, there is a lack in standardization for higher harmonics.

To evaluate the installation, the grid operator has to define a harmonic voltage emission limit. This process is standardized in the IEC technical report 61000-3-6 [26]. CIGRE TB 468 [27] provides practical information regarding emission assessment methods. Establishing this emission limit is usually a two-stage process, starting with the specification of planning levels. Compliance with the planning level at the connection point on high voltage should guarantee compliance with the harmonic compatibility levels in the underlying medium- and low-voltage grids. It is the responsibility of the grid operator to choose this limit accordingly. Indicative values are given in [26].

In the next step, a share of the planning is assigned as the emission limit to the installation. The amount depends on the pre-existing background distortion and the optional connection of future distorting installations. For the latter, not only the connection point under evaluation but also adjacent nodes in the grid have to be considered. As the allocation key, the agreed power of the installations can be used. In this process, it is important to take into account the variation in the harmonic phase angle. In practice, the total harmonic emission of several installations will not sum up linearly but geometrically. Since the actual phase angles are usually not known in advance, Ref. [26] provides a statistical approach, defining a general summation law. Depending on the harmonic order, α is selected according to Table 2.

$$U_{\mathrm{h,total}} = \sqrt[\alpha]{U_{\mathrm{h},i}^{\alpha}} \tag{5}$$

where

$U_{\mathrm{h,total}}$ total level for harmonic order h;
$U_{\mathrm{h},i}$ individual level for harmonic order h;
α summation exponent;
h harmonic order.

Table 2. Summation exponents for harmonics.

Harmonic Order	α
$h < 5$	1
$5 \leq h \leq 10$	1.4
$h > 10$	2

The other important part is the estimation of the harmonic emission of the new installation. This is based on the harmonic grid impedance on the one hand and on the harmonic currents of the installation on the other hand.

$$\underline{U}_{\mathrm{h},i} = \underline{Z}_{\mathrm{h},i} \cdot \underline{I}_{\mathrm{h},i} \tag{6}$$

where

$\underline{U}_{\mathrm{h},i}$ harmonic emission of installation i;
$\underline{Z}_{\mathrm{h},i}$ harmonic grid impedance at the point of connection;
$\underline{I}_{\mathrm{h},i}$ harmonic current of installation i.

The harmonic grid impedance can be calculated from the grid data for different system operating conditions considering peak and off-peak load scenarios and varying short-circuit capacities. The cable capacitance, reactive power compensation units, and filters must be taken into account, since they can cause resonance conditions and, thus, have a significant effect on the harmonic impedance. Loads should be modelled in an appropriate way because of their influence on resonance damping. Furthermore, the increase in resistance with increasing frequency due to the skin effect and proximity effect should be included in the model as it has an impact on damping as well. However, with usual available data the accuracy of the calculated impedance will decrease with higher frequencies. Especially the damping of resonances, affecting the magnitude of the impedance, might differ significantly from reality.

In Figure 9, an example of a simulated harmonic grid impedance is shown.

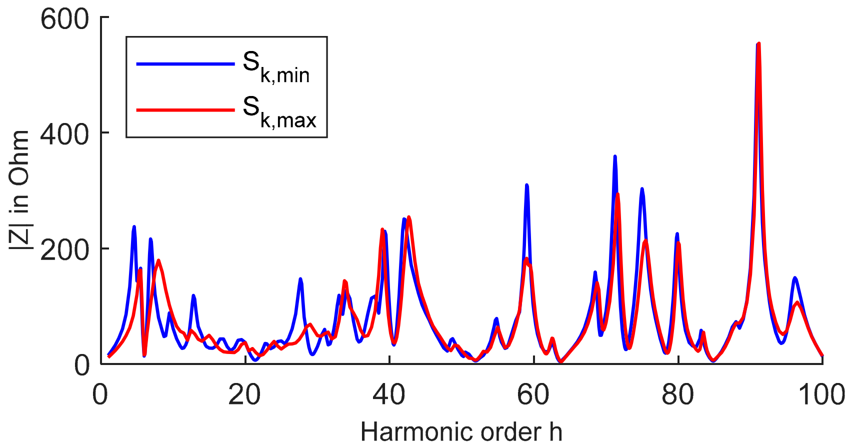

Figure 9. Amplitude of the harmonic grid impedance, evaluated at the PCC at 380 kV busbar in substation UW Kaprun for minimal (10.8 GVA) and maximal (13.5 GVA) short-circuit powers.

Equation (5) requires the installation to be specified as harmonic current source. This is fairly true for thyristor-based line-commutated converters (LCCs). In practice, for most applications an LCC equals a current source converter, justifying the modeling of it as current source. Modern devices are designed as voltage source converters (VSCs), behaving rather as a harmonic voltage source at the power electronic terminals. However, considering the impedance of the coupling reactance and the generator transformer, and assuming that they are significantly larger than the grid impedance, the modeling approach as a current source is reasonable as long as no serial grid resonances occur in the considered frequency range.

Thus, for assessment of the harmonic emission, the manufacturer has to provide measurement or simulation of the converter harmonic currents at the PCC or the converter harmonic voltages at the converter clamps and the relevant connection impedances to the PCC. The data have to include the influence of relevant switching patterns and different operating points (no load, partial load, full load). If relevant, inter-harmonic currents should be provided as well.

With all this information available the harmonic voltage emission can be calculated and compliance with given emission limits can be assessed.

5. Harmonics in the CFSM System

The three-level voltage source converter acts on the grid and on the machine side as a voltage source with a harmonic spectrum depending on the pulse pattern. The current harmonic spectrum results from the voltage harmonics and the effective impedance. Hence, the voltage and current harmonics at the single main parts of the CFSM system have to be evaluated independently. In the following, the occurring harmonics up to the 100th harmonic are discussed based on measurement results. These harmonics are important for grid compliancy and the evaluation of potential heating issues, loss distribution in the CFSM system, and pulsating torques.

The main focus on the generator-side converter is on the current harmonics since they lead to additional losses and a changed loss distribution in the generator and cause pulsating torques. In Figure 10, a simplified circuit diagram of the converter–generator connection is given. The converter is connected to the generator via an isolated phase bus (IPB).

For the interpretation of harmonic measurements, the total harmonic distortion of the current, THD_{i}, is calculated with the rated current, I_{N}, in the denominator. The resulting value corresponds to the total demand distortion (TDD), defined in [28].

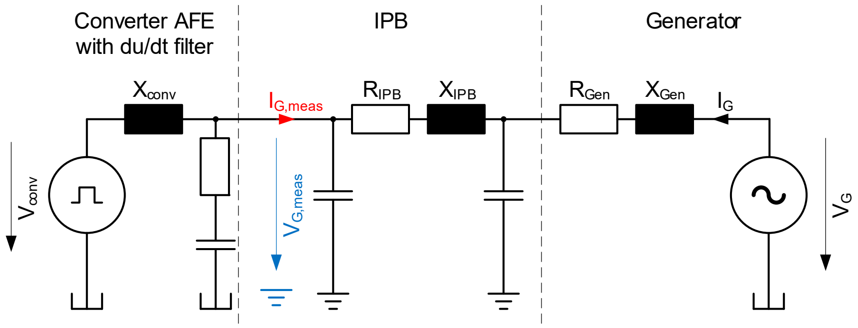

Figure 10. Converter–generator connection with measurement placement. R_{IPB} and X_{IPB} are the resistance and inductance of the IPB, and R_{Gen} and X_{Gen} are the stator resistance and inductance of the generator.

The THD_i of the measured generator current is given in Figure 11. The THD_i shows little dependency on the active power but is significantly reduced with an increased number of pulses. The THD_u on the other hand reduces with increased active power and has only a negligible dependency on the number of pulses. The reduction in THD_u is mainly caused by the increased generator voltage and, thus, the increased fundamental voltage U_1. The generator is operated at a power factor of 1. The THD values are calculated according to [26], Equations (7) and (8).

$$THD_i = \sqrt{\sum_{h=2}^{100} \left(\frac{I_h}{I_N} \right)^2} \tag{7}$$

$$THD_u = \sqrt{\sum_{h=2}^{100} \left(\frac{U_h}{U_1} \right)^2} \tag{8}$$

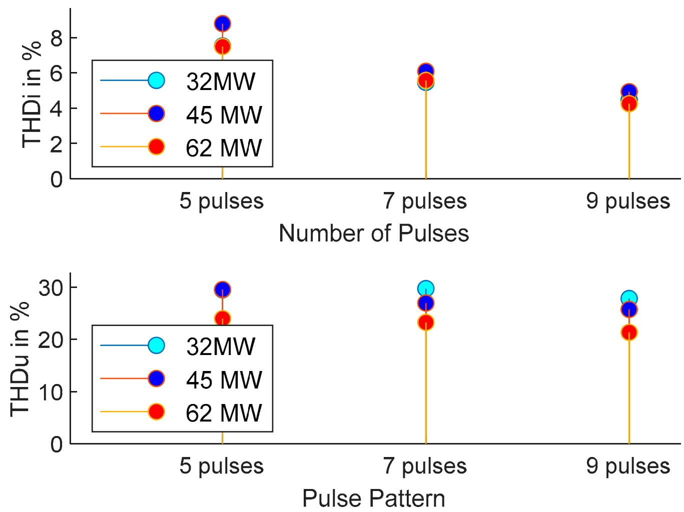

Figure 11. THD_i and THD_u (%), the nominal current and fundamental voltage, respectively.

To analyze the THD_i's behavior, a closer look has to be taken at the effective impedance, $\underline{Z}_{CG}$, between the converter output voltage and the internal generator voltage. The capacitive elements of the generator and the isolated phase bar, as well as the du/dt filter of the converter, can be neglected for frequencies up to the 100th harmonic. Thus, the effective impedance becomes ohmic-inductive and the generator current is calculated as

$$\underline{I}_{\mathrm{G}} = \frac{\underline{V}_{\mathrm{conv}} - \underline{V}_{\mathrm{G}}}{R_{\mathrm{IPB}} + R_{\mathrm{Gen}} + j\left(X_{\mathrm{conv}} + X_{\mathrm{IPB}} + X''_{\mathrm{Gen}}\right)} = \frac{\underline{V}_{\mathrm{conv}} - \underline{V}_{\mathrm{G}}}{\underline{Z}_{\mathrm{CG}}} \tag{9}$$

Assuming the generator voltage, $\underline{V}_{\mathrm{G}}$, is close to ideal, with negligible small harmonics, the current harmonics, $\underline{I}_{\mathrm{G},h}$, become a function of $\underline{Z}_{\mathrm{CG}}(f)$ and the harmonics of the converter voltage, $\underline{V}_{\mathrm{conv},h}$. The harmonic impedance of the generator can be assumed, according to [29], as the mean value of the sub-transient direct and quadrature inductances multiplied by the harmonic order, Equation (10).

$$X''_{\mathrm{Gen},h} = \frac{h}{2} \cdot \left(X''_{\mathrm{d}} + X''_{\mathrm{q}}\right) \tag{10}$$

This simplification neglects the effects of eddy currents and the conversion of harmonics into neighboring harmonics due to salient rotors. Further, the ohmic part of $\underline{Z}_{\mathrm{CG}}$ is neglected for the calculation of the current harmonic. This simplification is justified by the short length of the IPB, of around 3 m, and an X/R ratio greater than 50 for the generator. A detailed derivation of the harmonic generator impedance can be found in [30].

$$\underline{I}_{\mathrm{G},h} \sim \frac{\underline{V}_{\mathrm{conv},h}}{h \cdot j\left(X_{\mathrm{conv}} + X_{\mathrm{IPB}}\right) + jX''_{\mathrm{Gen},h}} \tag{11}$$

The harmonics of the converter voltage occur at the frequency f_{c} of the triangular reference function, its multiples, and at their odd side bands. For the used discontinuous pulse pattern, f_{c} is calculated from the number of pulses, x, and the fundamental frequency, f_1, as

$$f_{\mathrm{c}} = 3 \cdot x \cdot f_1 \tag{12}$$

fc and its multiples correspond to a zero-sequence system. Since the generator windings are y-connected with isolated star point current, harmonics can only occur on the side bands of fc building positive- and negative-sequence systems.

Figure 12a shows the harmonic spectra for five, seven, and nine pulses at a fixed power of 62 MW. The measurements were conducted at one stable operation point with subsequent changes in the number of pulses causing the generator voltage and power to be constant. The variation in the generator frequency at a stable active power setpoint, caused by slow oscillations of the hydraulic system, is also negligible; see Table 3. Thus, the modulation index is also constant for all three datasets, leading to constant amplitudes of the characteristic converter harmonics. The amplitude of the current harmonics decrease with higher numbers of pulses due to the higher order of the characteristic converter harmonics and, consequently, higher effective impedance; see Equations (11) and (12).

Table 3. Fundamental generator frequency in Hz for the evaluated operation points.

		Number of Pulses		
		5 Pulses	**7 Pulses**	**9 Pulses**
Active Power	32 MW	36.40	36.60	36.20
	45 MW	37.40	37.80	37.60
	62 MW	39.80	39.60	40.20

Figure 12b shows the dependency of the current harmonics in respect to different active power setpoints for five pulses. The active power is mainly controlled via the phasor angle of the fundamental voltage. The amplitudes of the voltage harmonics are only slightly influenced by the active power setpoints due to changes in the frequency and amplitude of the generator voltage causing small changes in the modulation index. Thus, the current harmonics are nearly independent of the active power setpoint. In Figure 12b, the harmonic currents are shown as absolute values to highlight this independence.

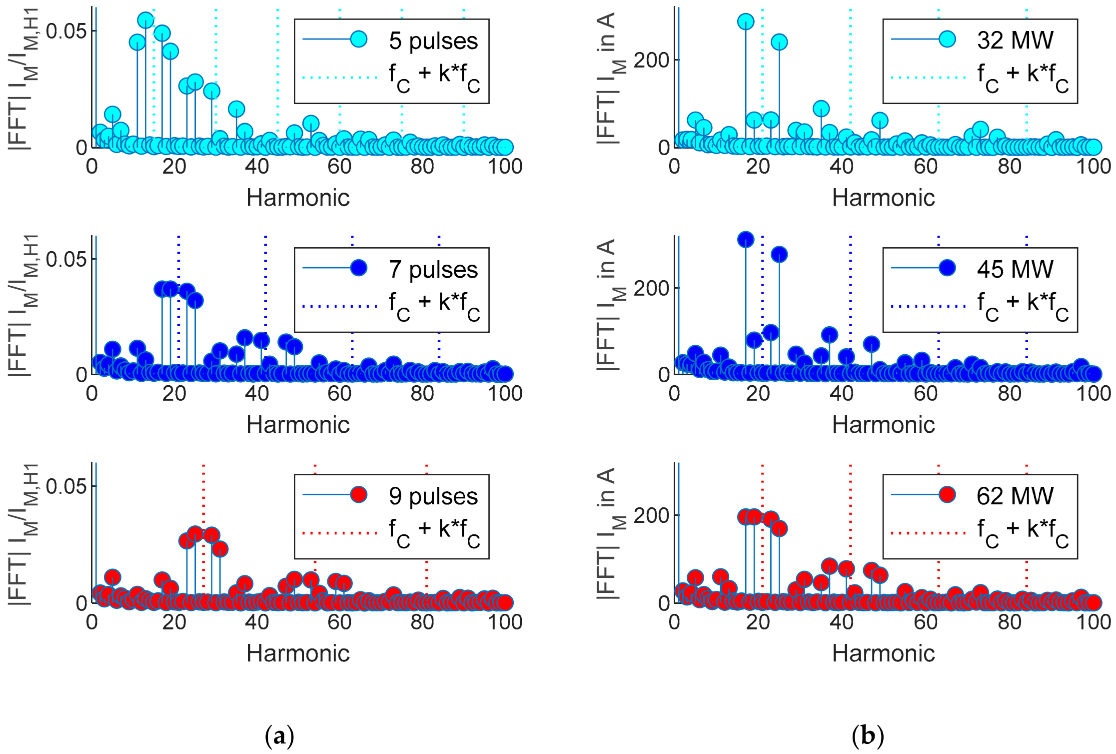

Figure 12. (**a**) Current harmonics, in pu, of the rated generator current for different number of pulses at 62 MW. (**b**) Current harmonics in absolute values for different active power operation points and x = 5 pulses.

The fundamental generator frequencies, and hence the speed of the generator, for the evaluated operation points are given in Table 3 for the sake of completeness.

The grid side of the converter uses a pulsing pattern with x = 5 pulses over the complete operational area. Therefore, the harmonics are nearly independent from the operation point. The mean value over the nine measurements of the total current and voltage harmonic distortions at the low-voltage side of the transformer are THD_{i} = 4.75% and THD_{u} = 10.84%. The harmonics in the current and voltage are reduced by the 5-winding transformer connecting the converter to the 110 kV grid, resulting in total current and voltage harmonic distortions of THD_{i} = 1.92% and THD_{u} = 1.69% on the high-voltage side of the transformer. The current and voltage curves on the low-voltage and high-voltage sides of the transformer are shown in Figure 13.

The reduction in the voltage harmonics is caused by two main effects. The first is the interleaving pulses of the four converter units, leading to the resulting line-to-line voltage shown in Figure 5. The second effect is a harmonic voltage drop over the transformer. The transformer impedance between the 110 kV winding and each parallel 6.4 kV winding is 0.28 pu at a rated power of 21.25 MVA. The short-circuit power of the grid at the 110 kV level is around 1.15 GVA, with only a small dependency on the load case of the transmission grid. Assuming an ideal voltage source at the grid without any voltage harmonics, the transformer impedance and the grid impedance represent a voltage divider for the converter-caused voltage harmonics, whereby the transformer impedance is dominant.

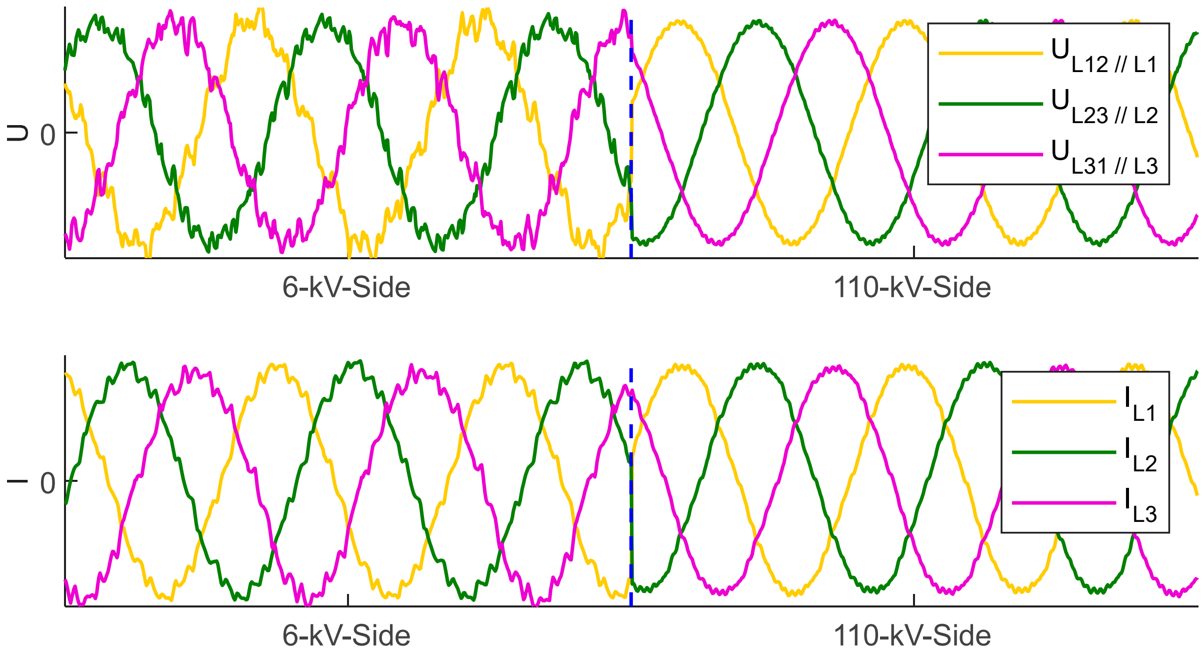

Figure 13. Current and voltage curves at the transformer windings. Left: at converter side; Right: at grid side.

6. Shaft Voltage and Bearing Current

The shaft voltage, and as a consequence bearing currents, is a well-known phenomenon in rotating AC machines [31,32]. There are a variety of reasons that can be described by different mechanisms. The reasons for the shaft voltage in AC machines operated at power frequencies are typically the magnetic asymmetry of the magnetic circuit or the electrostatic charge due to friction [33]. Additional mechanisms are effective in converter-fed AC machines. Common-mode voltages lead to a current that flows from phases into the earthing system of the power plant [34]. The couple path of these common-mode currents are the stray capacitance between the stator windings and the rotor $C_{SW\text{-}R}$ as well as the stator windings to stator $C_{SW\text{-}SP}$, as shown in Figure 14 [34]. A further mechanism is given by the high-frequency common-mode current i_C that flows from the stator windings to the connection between the stator and the power plant's earthing system. These currents lead to a tangential magnetic flux, Φ_C, and an induced shaft voltage (vs.) (Figure 14) [32,35,36].

Voltage measurements at the no-driven side of the shaft referred to power plant earthing system show a bearing voltage, v_b, with a synchronous part corresponding to the generator fundamental frequency and high-frequency peaks, with a voltage maximum of $\pm$400 V (Figure 15). The driven side of the shaft is earthed and the bearing voltage is equal to the shaft voltage (vs.). The shaft voltage (vs.) causes capacitive currents at the bearings and can lead to partial or full discharges at the electric insulation (e.g., oil film). The electric stress can be reduced by bridging the insulation.

The peak values of the shaft voltage can be lowered by earthing the non-driven side of the shaft with a brush and a capacitance C_{EB} (Figure 16a). The capacitance forms, with the stray capacitance between the stator winding and the rotor $C_{SW\text{-}R}$, a capacitive divider. The higher the earthing capacity compared to the stator winding and rotor capacity, the lower the proportion of the common-mode voltages at the shaft. The peak values of the shaft voltage can be reduced by 100 V with a capacitance, C_{EB}, of 4.7 µF (Figure 16b).

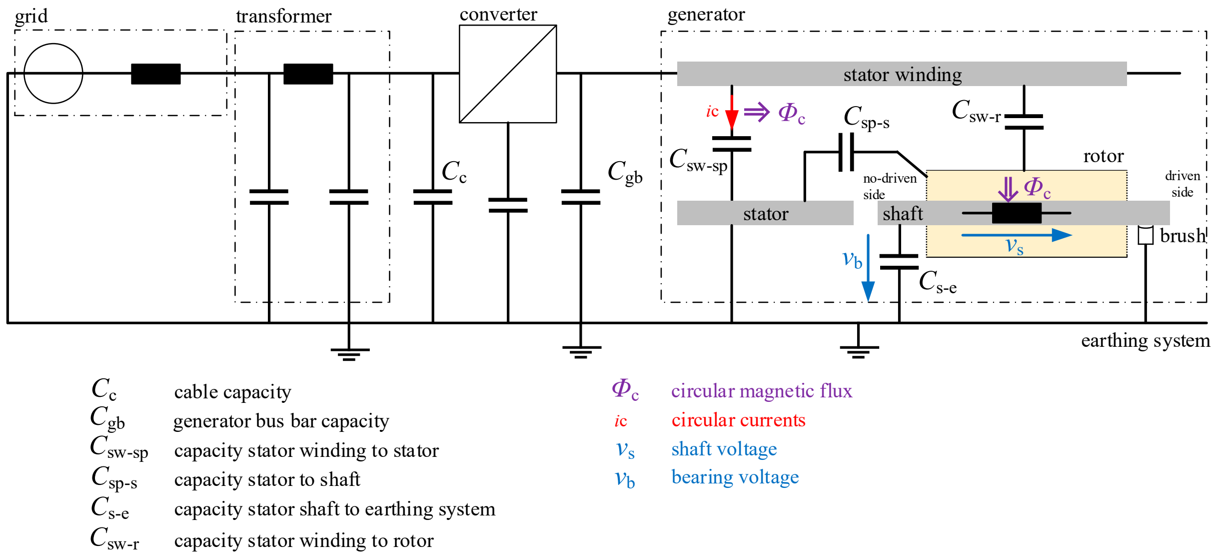

Figure 14. Simplified equivalent circuit of shaft voltage v_s induced by capacitive coupling and circular currents of the converter-fed generator of the pumped-storage power plant.

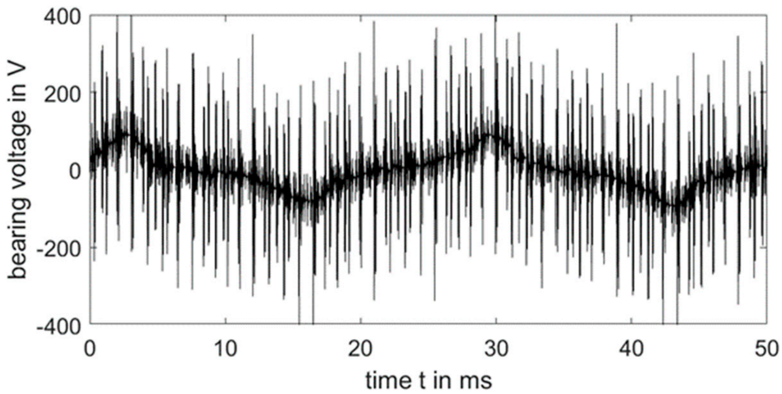

Figure 15. Bearing voltage measured (measuring equipment: active probe Pico Technology TA041 and Oscilloscope Rohde and Schwarz RTH1004) at the non-driven side of the shaft at the generator of machine 1 (operation point: 15 MW, asynchron, H3, 350 Hz).

A parallel resistor, R_{EBP} (to avoid electrostatic charges) and a serial resistor, R_{EBS} (to limit the maximum leakage currents) are additionally connected to the earthing capacity. It can be clearly seen that a capacitive current with peak values up to 10 A flowed in the earthing capacity (Figure 16c). The synchronous shaft voltage leads to a resistive current (Figure 16d).

It seems that the shaft voltage caused by the tangential magnetic flux, Φ_C, cannot be reduced considerably by capacitive earthing of the non-driven side of the shaft. A resistive earthing of the non-driven side leads to high shaft currents depending on the chosen resistor. Conventional shaft current transformers as protective devices should be evaluated because high-frequency shaft currents cannot be measured or cannot be measured correctly.

Further measures to reduce shaft voltage can be proposed, like a reduction in the voltage-rise rate of the converter by an output filter. Otherwise, the components at the power unit have been dimensioned to handle these shaft voltages with high amplitudes and frequencies.

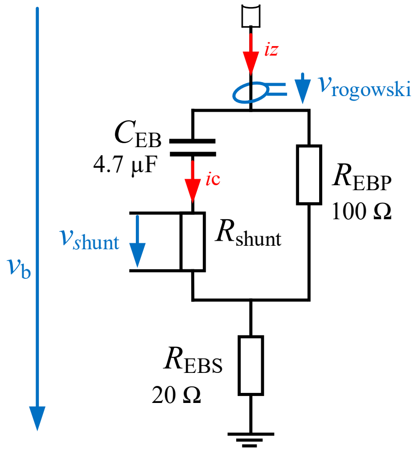

(**a**)

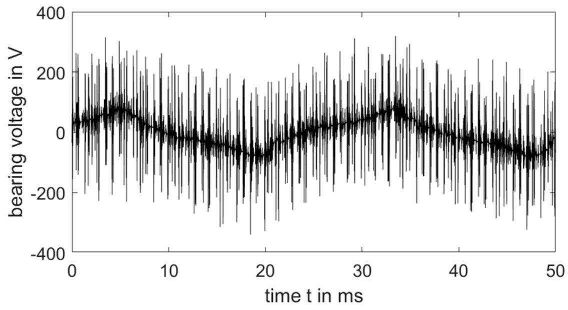

(**b**) Measuring equipment: active probe Pico Technology TA041 and Oscilloscope Rohde and Schwarz RTH1004

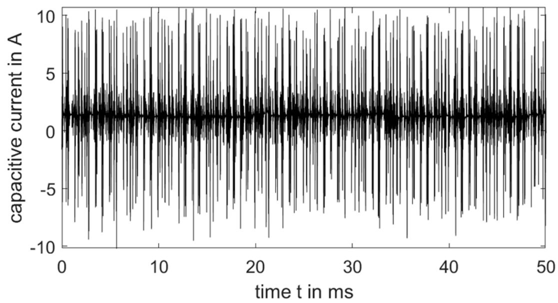

(**c**) Measuring equipment: resistive shunt 75 mV/2A, active probe Pico Technology TA041 and Oscilloscope Rohde and Schwarz RTH1004

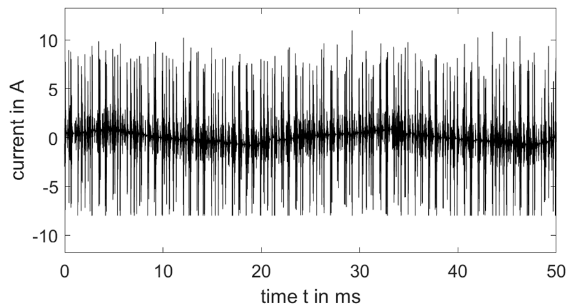

(**d**) Measuring equipment: Rogowski current probe Chauvin Arnoux MA200-70 and Oscilloscope Rohde and Schwarz RTH1004

Figure 16. (**a**) Equivalent circuit of earthing capacity C_{EB}, the parallel resistor R_{EBP}, the resistive shunt R_{shunt}, and the current-limiting resistor in series R_{EBS}, as well as the capacitive displacement current i_{cap}, the total leakage current i_{z}, the Rogowski current probe output voltage v_{rogowski}, and the shunt voltage v_{shunt}. (**b**) Bearing voltage v_{b}, (**c**) capacitive displacement current i_{cap}, and (**d**) total leakage current i_{z} measured at the non-driven shaft end (C_{EB} = 4.7 µF, R_{EBS} = 20 Ω, R_{EBP} = 100 Ω).

7. Conclusions

The analyses and measurement evaluations in this paper highlight the practical electrical challenges of large-scale CFSM which have to be considered in the design phase of such systems. The robust converter solution with high power density implemented successfully in Limberg I has been presented and analyzed.

Focusing on the effects of different pulse patterns in Section 2, it becomes obvious, that the selection of the number of pulses per half wave needs a careful evaluation of the harmonic effects in the CFSM system. The optimization process has to consider the allowed harmonic emission to the grid, the switching-related converter losses and the $\mathrm{THD_i}$ at the motor–generator. This optimization process led to the choice of a higher number of pulses in Limberg I and, thus, shifting losses from the generator to the converter.

Section 3 discussed a typical voltage–current profile at the motor generator for variable-speed operation. The DC to low-frequency currents and voltages occurring during start-up are a critical design criterion affecting the measurement transducers and generator.

The large-scale converters used in the CFSM system can cause significant harmonic emission. The harmonic emission must be considered already in an early design stage. The frequency-dependent impedance at the point of common coupling and the allowed emission level are necessary information that have to be provided by the grid operator. If the envelope curve of the voltage respectively current harmonics emitted at the converter clamps are known, an evaluation using suitable grid simulation software is possible. Special care has to be taken with resonances occurring between the converter clamps and the PCC.

The measurements in the CFSM system analyzed in Section 5 provide a validation of the simulations and design considerations. The results show the optimization potential of the voltage and current harmonics on the generator side.

Section 6 focuses on the evaluation of the shaft voltage and possible reduction measures. The principal occurrence of a voltage at the insulated bearing is not unknown in hydro generators. However, in classic configurations, a low-frequency voltage caused by magnetic asymmetries of the generator mainly appears. The shown high-frequency parts were so far studied in converter-fed drives, with powers in a range up to several hundred kilowatts. It is shown that the shaft voltage can be reduced by earthing the shaft with an RC circuit. Nevertheless, the shaft voltage remains quite high because of the induction by the tangential magnetic flux.

The described effects are well-known for converter-fed drives in lower-power applications, but are new challenges for large-scale hydro-power applications. Adapting known engineering practices to the higher power of variable-speed hydro leads to a very flexible power plant, which plays an important role in Verbund's generation fleet.

Author Contributions: Conceptualization, S.P. and J.D.; methodology, S.P., J.D. and M.J.; software, S.P., J.D. and M.J.; validation, S.P., J.D. and M.J.; formal analysis, S.P. and J.D.; investigation, S.P., J.D., M.J., H.R. and A.B.; resources, S.P., J.D., M.J., H.R. and A.B.; data curation, S.P. and J.D.; writing—original draft preparation, S.P., J.D., M.J., H.R. and A.B.; writing—review and editing, S.P.; visualization, S.P., J.D., M.J., H.R. and A.B.; supervision, S.P. and J.D.; project administration, S.P. All authors have read and agreed to the published version of the manuscript.

Funding: This research received no external funding.

Data Availability Statement: The data presented in this study are available on request from the corresponding author. The data are not publicly available due to privacy.

Conflicts of Interest: The authors declare no conflict of interest.

References

1. Kerkman, R.J.; Lipo, T.A.; Newman, W.G.; Thirkell, J.E. An inquiry into adjustable speed operation of a pumped hydro plant. Part 1—Machine design performance. *IEEE Trans. Power Appar. Syst.* **1980**, *PAS-99*, 1828–1837. [CrossRef]
2. Barros, J.G.C.; Saidel, M.A.; Ingram, L.; Westphalen, M. Adjustable Speed Operation of Hydroelectric Turbine Generators. *Electra* **1996**, *167*, 17–37.
3. Fraile-Ardanuy, J.; Wilhelmi, J.R.; Fraile-Mora, J.J.; Perez, J.I. Variable-speed Hydro Generation: Operational Aspects and Control. *IEEE Trans. Energy Convers.* **2006**, *21*, 569–574. [CrossRef]
4. Bortoni, E.; de Souza, Z.; Viana, A.; Villa-Nova, H.; Rezek, A.; Pinto, L.; Siniscalchi, R.; Braganca, R.; Bernardes, J. The Benefits of Variable Speed Operation in Hydropower plants Driven by Francis Turbines. *Energies* **2019**, *12*, 3719. [CrossRef]
5. Valavi, M.; Nysveen, A. Variable-Speed Operation of Hydropower Plants. *IEEE Ind. Appl. Mag.* **2018**, *24*, 18–27. [CrossRef]
6. Merino, J.M.; Lopez, A. ABB Varspeed generator boosts efficiency and operating flexibility of hydropower plant. *Fuel Energy Abstr.* **1996**, *3*, 33.
7. Sporild, R.; Gjerde, J.O.; Gjengedal, T. Improved System Performance by Integration of Adjustable Speed Hydro Machines. In Proceedings of the International Conference on Power System Technology, Perth, WA, Australia, 4–7 December 2000.
8. Wilhelmi, J.R.; Fraile-Ardanuy, J.J.; Fraile-Mora, J.J.; Inigo, L. Adjustable Speed Hydro Generation. Renew. *Energy Power Qual. J.* **2003**, *1*, 240–245. [CrossRef]
9. Mayrhuber, J.; Giefing, D.; Döltelmayer, R.; Ladreiter-Knauss, C. Upgrading of hydropower plants for the EU-Green Deal: Efficiency upgrade projects for more generation and flexibility. In Proceedings of the Hydro 2022, Strasbourg, France, 25–27 April 2022.
10. Reigstad, T.I.; Uhlen, K. Nonlinear model predictive control of variable speed hydropower for provision of fast frequency reserves. *Electr. Power Syst. Res.* **2021**, *194*, 107067. [CrossRef]
11. Mennemann, J.-F.; Marko, L.; Schmidt, J.; Kemmetmüller, W.; Kugi, A. Nonlinear Model Predictive Control of a Variable-Speed Pumped-Storage Power Plant. *IEEE Trans. Control Syst. Technol.* **2019**, *29*, 645–660. [CrossRef]
12. Reigstad, T.I.; Uhlen, K. Optimized Control of Variable Speed Hydropower for Provision of Fast Frequency Reserves. *Electr. Power Syst. Res.* **2020**, *189*, 106668. [CrossRef]

13. Nicolet, C.; Beguin, A.; Dreyer, M.; Alligne, S.; Jung, A.; Cordeiro, D.; Moreira, C. Inertia Emulation Contribution of Frades 2 Variable Speed Pump-Turbine to Power Network Stability. In Proceedings of the 21st Inern. Seminar on Hydropower Plants—Hydropower for Future Generations, Vienna, Austria, 9–11 November 2022.
14. Akbari, H.; Perez-Diaz, J.I.; Sarasua, J.-I.; Schürhuber, R. Implementation and Evaluation of a Complex Pumped-Storage Hydropower Plant with FOur Units, Common Penstock and Surge Tank in a REal-Time Digital Simulator. *Energies* **2023**, *16*, 3828. [CrossRef]
15. Reigstad, T.I.; Uhlen, K. Modelling of Variable Speed Hydropower for Grid Integration Studies. *IFAC-PapersOnLine* **2020**, *53*, 13048–13055. [CrossRef]
16. Bogenrieder, W.; Groschke, L. Design and Construction of Germany's Goldisthal Pumped-Storage Scheme. *Int. J. Hydro Power Dams* **2000**, *7*, 29–31.
17. Bocquel, A.; Janning, J. Analysis of a 300 MW variable speed drive for pump-storage plant applications. In Proceedings of the 2005 European Conference on Power Electronics and Applications, Dresden, Germany, 11–14 September 2005.
18. Koutnik, J.; Hildinger, T.; Martin, B. Ein Sprung nach vorn—Drehzahl-variables Pumpspeicherkraftwerk Frades II. *Wasserwirtschaft* **2015**, *105*, 27–32. [CrossRef]
19. Koutnik, J. Frades II-variable speed pumped storage project and its benefit to the electrical grid. *Proc. Int. Conf. Renew. Energy* **2012**, 1–7. [CrossRef]
20. Müller, U.; Marclay, R.; Hohberg, J.-M.; Hase, M. The Linth-Limmern hydro-power plant—Design and construction of a large pumped storage scheme. In Proceedings of the World Tunnel Congress 2013, Geneva, Switzerland, 31 May–7 June 2013.
21. Schlunegger, H. Pumping efficiency: A 100 MW converter for the Grimsel 2 pumped storage plant. *Environ. Sci.* **2014**, *1*, 42–47.
22. Häderli, C.; Thurnherr, T.; Christe, A.; Faulstich, A.; Ladreiter-Knauss, C. Project Malta Upper Stage—World's First Direct Modular Multilevel Converter for Variable-Speed PUmped Storage Hydropower. In Proceedings of the Hydro 2022 Conference, Strasbourg, France, 25–27 April 2022.
23. Aubert, S.; Häderli, C.; Ladreiter-Knauss, C.; Polster, S.; Steinmann, P. Malta Oberstufe Overhaul Project Variable Speed Operation With MMC Full Converter. In Proceedings of the Vienna Hydro 2022, Vienna, Austria, 9–11 November 2022.
24. Jakob, R.; Keller, C.; Möhlenkamp, G.; Gollentz, B. 3-Level high power converter with press pack IGBT. In Proceedings of the 2007 European Conference on Power Electronics and Applications, Aalborg, Denmark, 2–5 September 2007.
25. Brückner, T. *The Active NPC Converter for Medium Voltage Drives*; Shaker Verlag GmbH: Dresden, Germany, 2006.
26. *IEC/TR 61000-3-6 2008-02*; Electromagnetic Compatibility (EMC)—Part 3–6: Limits—Assessment of Emission Limits for the Connection of Distorting Installations to MV, HV and EHV Power Systems. IEC: Geneva, Switzerland, 2008.
27. *C. W. C4.109*; Review of Disturbance Emission Assessment Techniques. CIGRE: Paris, France, 2011.
28. *IEEE Std 519*; IEEE Recommended Practice and Requirements for Harmonic Control in Electric Power Systems. IEEE: Piscataway, NJ, USA, 2014.
29. Adkins, B.; Harley, R.G. *The General Theory of Alternating Current Machines: Application to Practical Problems*; Springer: Dordrecht, The Netherlands, 1975.
30. Eggleston, J.F. *Harmonic Modelling of Transmission Systems Containing Synchronous Machines and Static Convertors*; Unversity of Canterbury: Christchurch, NZ, USA, 1985.
31. Tischmacher, H. Systemanalysen zur Elektrischen Belastung von Wälzlangern bei Umrichtergespeisten Elektromotoren. Ph.D. Thesis, Gottfried Wilhelm Leibniz Universität Hannover, Hannover, Germany, 2017.
32. Zhu, W.; De Geatano, D.; Chen, X.; Jewell, G.W.; Hu, Y. A Review of Medling and Mitigation Technicques for Bearing Currents in Elekctrical Machines with Variable Freqency Drives. *IEEE Acess* **2022**, *10*, 125279–125297. [CrossRef]
33. Ammann, C.; Reichert, K.; Joho, R.; Posedel, Z. Shaft Voltages in Generators with Static Excitation System Problems and Solution. *IEEE Trans. Energy Convers.* **1988**, *3*, 409–419. [CrossRef] [PubMed]
34. Chen, S.; Lipo, T.A.; Fitzgerald, D. Source of Induction Motor Bearing Currents caused by PWM Inverters. *IEEE Trans. Energy Convers.* **1996**, *11*, 25–32. [CrossRef]
35. Mütze, A.; Binder, A. Calculation of the Influence of Insulated Bearings and Insulated Inner Bearing Seats on Circulating Bearing Currents in Machines of Inverter-Based Drive Systems. In Proceedings of the IEEE International Conference on Electric Machines and Drives, San Antonio, TX, USA, 15 May 2005.
36. Chen, S.; Lipo, T.A.; Novotny, D.W. Circulating Type Motor Bearing Current in Inverter Drives. In Proceedings of the IAS '96. Conference Record of the 1996 IEEE Industry Applications Conference Thirty-First IAS Annual Meeting, San Diego, CA, USA, 6–10 October 1996.